SCIENCE CHINA
Earth Sciences

•RESEARCH PAPER•

March 2021 Vol.64 No.3: 377–387
https://doi.org/10.1007/s11430-020-9686-0

Seismic wave equations in tight oil/gas sandstone media

Jinghuai GAO[1,2*], Weimin HAN[5], Yanbin HE[4], Haixia ZHAO[3], Hui LI[1,2], Yijie ZHANG[1,2] & Zongben XU[3]

[1] *School of Electronic and Information Engineering, Xi'an Jiaotong University, Xi'an 710049, China;*
[2] *National Engineering Laboratory of Offshore Oil Exploration, Xi'an 710049, China;*
[3] *School of Mathematics and Statistics, Xi'an Jiaotong University, Xi'an 710049, China;*
[4] *School of Mechanical Engineering, Xi'an Jiaotong University, Xi'an 710049, China;*
[5] *Department of Mathematics, University of Iowa, Iowa 52242, USA*

Received January 11, 2020; revised September 3, 2020; accepted September 27, 2020; published online December 16, 2020

Abstract Tight oil/gas medium is a special porous medium, which plays a significant role in oil and gas exploration. This paper is devoted to the derivation of wave equations in such a media, which take a much simpler form compared to the general equations in the poroelasticity theory and can be employed for parameter inversion from seismic data. We start with the fluid and solid motion equations at a pore scale, and deduce the complete Biot's equations by applying the volume averaging technique. The underlying assumptions are carefully clarified. Moreover, time dependence of the permeability in tight oil/gas media is discussed based on available results from rock physical experiments. Leveraging the Kozeny-Carman equation, time dependence of the porosity is theoretically investigated. We derive the wave equations in tight oil/gas media based on the complete Biot's equations under some reasonable assumptions on the media. The derived wave equations have the similar form as the diffusive-viscous wave equations. A comparison of the two sets of wave equations reveals explicit relations between the coefficients in diffusive-viscous wave equations and the measurable parameters for the tight oil/gas media. The derived equations are validated by numerical results. Based on the derived equations, reflection and transmission properties for a single tight interlayer are investigated. The numerical results demonstrate that the reflection and transmission of the seismic waves are affected by the thickness and attenuation of the interlayer, which is of great significance for the exploration of oil and gas.

Keywords Tight oil/gas, Wave equation, Porosity, Permeability, Physical parameter, Complete Biot's equations, Volume-averaging technique

Citation: Gao J, Han W, He Y, Zhao H, Li H, Zhang Y, Xu Z. 2021. Seismic wave equations in tight oil/gas sandstone media. Science China Earth Sciences, 64 (3): 377–387, https://doi.org/10.1007/s11430-020-9686-0

1. Introduction

Tight oil/gas is an important type of resource, which is widely distributed in many parts of the world in different forms such as tight sandstone oil and gas reservoirs, shale oil and gas reservoirs and etc. Compared with that of the conventional two-phase media, the matrix and saturated fluid of tight oil/gas have special features (Wang, 2013; Kang, 2016). Wave propagation theory in multi-phase media is the theoretical foundation for the tight oil and gas exploration. Two approaches have been adapted in the development of the wave propagation theory in multi-phase media (Pride et al., 1992). One approach is through an application of the theory of macroscopic continuum mechanics on observable macroscopic quantities. The other approach is to derive the macroscopic motion equations using the volume averaging technique, starting with the microscopic equations for the fluid and solid grains.

Biot's theory or Biot's model is based on the first approach

* Corresponding author (email: jhgao@xjtu.edu.cn)

(Biot, 1956a, 1956b) which is one of the most fundamental wave propagation theories in porous media and has been applied widely. Biot's theory describes the wave propagation in fluid-saturated porous media. In Biot's theory, it is assumed that effects at the microscopic level can be ignored, and the theory of continuum mechanics can be applied to the measurable macroscopic quantities; then the governing equations of wave propagation are derived from the Lagrangian equations. Biot's theory predicted the existence of three types of waves in porous media: fast P wave, slow P wave and S wave. The theoretical prediction was confirmed by experiments which validated the Biot's theory. In 1962, Biot investigated the acoustic wave propagation in porous media and extended the theory to cover heterogeneous, anisotropic and viscoelastic media. Thus, the prototype of wave propagation theory in viscoelastic porous media was established (Biot, 1962). Based on the theory of irreversible thermodynamics and viscoelasticity, Biot (1973) further developed a theory for nonlinear and semilinear mechanics of porous solids.

However, it was found that Biot's theory could not be used to explain the dispersion and attenuation of waves in ultrasonic frequency band. In order to overcome this difficulty, a new model known as Biot and squirt flow (BISQ) model was proposed (Johnston et al., 1979; Winkler, 1985; Sams et al., 1997). It was also found that Biot's theory could not be used to describe the attenuation phenomenon in seismic frequency band; consequently, the patchy model was proposed (Mavko et al., 1998).

Parra (1997) extended the BISQ theory for non-isotropic media, and analyzed the dispersion of velocity and wave attenuation in the media. Diallo and Appel (2000) modified the BISQ theory, in which the fluid pressure is independent of the squirt flow length. Diallo et al. (2003) used the pulse transmission technique to measure the velocity and attenuation of ultrasonic P and S waves from two sets of rock samples. From experimental results on the velocity and attenuation, it was found that the modified BISQ model provided better numerical prediction than the BISQ model. Cheng et al. (2002) extended the BISQ model for viscoelastic media.

We now briefly review the literature on wave propagation theories in porous media based on the second approach. de La Cruz and Spanos (1985) proposed a complete system of equations that describes the seismic wave propagation at a low frequency in porous media filled with fluid. The method was based on volume-averaging, combined with an order-of-magnitude analysis and physical argument. They obtained equations similar in form to Biot's equations, and were able to relate the parameters in Biot's theory to physical quantities. Taking the thermal effect into consideration on mechanical motions, de La Cruz and Spanos (1989) applied the volume-averaging technique to derive the governing equations in fluid-filled porous media. Pride et al. (1992) derived linear dynamic equations and a stress-strain relation in isotropic two-phase (solid and fluid) media using the volume-averaging technique. The macroscopic equations matched the equations of motion and the stress-strain relation in Biot's theory. The effective fluid density is clearly defined with the tractive effort on the interface between pores and fluid (the wall of pores). Cruz et al. (1993) investigated the equilibrium thermodynamics in porous media based on the volume-averaging technique. Sahay et al. (2000) considered porous media composed of interconnected pores and chemically inserted viscous fluid. Macroscopic constitutive equations in heterogeneous anisotropic porous media were derived by averaging the constitutive equations at the pore scale, and a relationship between these equations and the corresponding equations in Biot (1962) was established. Sahay (2001) investigated the seismic wave propagation in heterogeneous isotropic media, and developed the macroscopic equations of motion and constitutive equations in heterogeneous isotropic media. In the most general case, there are twenty-seven independent parameters in the equations. In 2002, Spanos and Udey derived the complete Biot's theory, taking into consideration of diffusion and inertial terms through the volume-averaging technique. Unlike the classical Biot's theory, in the complete Biot's theory, the porosity is taken as a state variable, depending on both the temperature and time (de La Cruz and Spanos, 1985; Hickey et al., 1995; Spanos et al., 2002). Spanos (2009) investigated the seismic wave propagation in the combinatorial elastic media using volume-averaging.

In summary, much work has been done in the investigation of the porous media and various equations were proposed. These equations are complicated and contain numerous parameters. In applications, it is required to solve corresponding inverse problems of these equations which represents a very challenging task. For the particular case of oil and gas reservoirs, we may focus on the principal factors and ignore the secondary factors in order to reconstruct the physical parameters of the underground. Using the simplified equations to reconstruct the parameters appears to be a feasible approach (Bourbié et al., 1987). Motivated by this consideration, in this paper, we derive seismic wave equations for tight oil and gas media.

2. "Complete Biot's theory" in porous medium

2.1 Microscopic motion equations in fluid and solid, volume averaging theorem, micro-scale motion equation of fluid and solid

2.1.1 Microscopic motion equations in fluid and solid

The stress-strain relation of pore fluid is (Zhao and Liao, 1983; Landau and Lifshitz, 1987)

$$\sigma_{ij}^{\mathrm{f}}=\mu_{\mathrm{f}}\left(v_{i,j}^{\mathrm{f}}+v_{j,i}^{\mathrm{f}}-\frac{2}{3}v_{l,l}^{\mathrm{f}}\delta_{ij}\right), \tag{1}$$

where σ_{ij}^{f} is the stress tensor of the fluid, μ_{f} is the dynamic viscosity coefficient, $v_{i,j}^{\mathrm{f}}=\frac{\partial v_i^{\mathrm{f}}}{\partial x_j}$, and $v_i^{\mathrm{f}}$is the ith component of the fluid velocity v^{f}. δ_{ij} is the Kronecker Delta symbol.

The momentum flux density of a viscous fluid can be expressed as (Landau and Lifshitz, 1959)

$$\Pi_{ij}=p^{\mathrm{f}}\delta_{ij}+\rho_{\mathrm{f}}v_i^{\mathrm{f}}v_j^{\mathrm{f}}-\sigma_{ij}^{\mathrm{f}}, \tag{2}$$

where p^{f} is the fluid pressure and ρ_{f} is the density of the fluid.

The Euler equation is written as

$$\frac{\partial}{\partial t}\rho_{\mathrm{f}}v_i^{\mathrm{f}}=-\frac{\partial\Pi_{ij}}{\partial x_j}. \tag{3}$$

Substituting eq. (2) into eq. (3), we obtain the motion equation of the fluid

$$\frac{\partial}{\partial t}\rho_{\mathrm{f}}v_i^{\mathrm{f}}+\frac{\partial}{\partial x_j}\left(p^{\mathrm{f}}\delta_{ij}+\rho_{\mathrm{f}}v_i^{\mathrm{f}}v_j^{\mathrm{f}}-\sigma_{ij}^{\mathrm{f}}\right)=0. \tag{4}$$

2.1.2 *Micro-scale motion equation of elastic solid*

If the thermal effect can be ignored in the mechanical process, and the body force and gravity are negligible, the motion equation of a solid particle can be written as

$$\rho_{\mathrm{s}}\frac{\partial}{\partial t}u_i^{\mathrm{s}}=\frac{\partial\sigma_{ij}^{\mathrm{s}}}{\partial x_j}, \tag{5}$$

where u_i^{s} is the ith component of the displacement vector $\mathbf{u}^{\mathrm{s}}$ of the solid, ρ_{s} is the mass density of the solid, and $\sigma^{\mathrm{s}}=\left(\sigma_{ij}^{\mathrm{s}}\right)$ is the stress tensor of the solid. For linear elasticity with isotropic material (Mase and Mase, 2001), we have

$$\sigma_{ij}^{\mathrm{s}}=K_{\mathrm{s}}u_{ll}^{\mathrm{s}}\delta_{ij}+2\mu_{\mathrm{s}}\left(u_{ij}^{\mathrm{s}}-\frac{1}{3}\delta_{ij}u_{ll}^{\mathrm{s}}\right), \tag{6}$$

where K_{s} is the bulk modulus of the solid, μ_{s} is the shear modulus of the solid, and u_{ij}^{s} is defined as

$$u_{ij}^{\mathrm{s}}=\frac{1}{2}\left(u_{i,j}^{\mathrm{s}}+u_{j,i}^{\mathrm{s}}\right). \tag{7}$$

2.1.3 *The fluid-solid interface condition*

Assuming that there is no slip on the interface of the fluid and the solid (de la Cruz and Spanos, 1985), we have

$$\vec{v}^{\mathrm{f}}=\frac{\partial\vec{u}^{\mathrm{s}}}{\partial t}. \tag{8}$$

Assuming that the normal stress of the solid and the fluid is continuous across the interface, we have

$$-p^{\mathrm{f}}n_i+\sigma_{ij}^{\mathrm{f}}n_j=\sigma_{ij}^{\mathrm{s}}n_j, \tag{9}$$

where n=(n_i) is the normal unit vector of the interface. Eqs. (8) and (9) are the interface conditions between the fluid and the solid.

2.1.4 *Volume averaging and phase averaging*

Let V be a sub-region in the porous medium and assume that all of the sub-regions have similar shapes, volumes, and directions. In this paper, V is defined as a sphere or cuboid with the bary-centric point$\vec{x}$, i.e., $V=B(\vec{x};r)$ for a sphere with radius r centered at $\vec{x}$, and $V=B\left(\vec{x};l_1,l_2,l_3\right)$ for a cuboid, l_1, l_2, and l_3 being the lengths of three sides and the characteristic length is max $\{l_1, l_2, l_3\}$.

Let $G^{\mathrm{f}}(\vec{x}')$ be a physical quantity related to the fluid that is defined as zero outside of the fluid region. There are two kinds of averages: bulk average and phase average. The bulk average of $G^{\mathrm{f}}(\vec{x}')$ over V is defined as

$$\left\langle G^{\mathrm{f}}\right\rangle=\frac{1}{V}\int_V G^{\mathrm{f}}(\vec{x}')\mathrm{d}V, \tag{10}$$

which is a function of $\vec{x}$. If the characteristic length of V is longer than the scale of the solid particle, the bulk average function can be considered continuous. The phase average of G^{f} is defined as

$$\overline{G}^{\mathrm{f}}=\frac{1}{V_{\mathrm{f}}}\int_V G^{\mathrm{f}}(\vec{x}')\mathrm{d}V, \tag{11}$$

where V_{f} represents the volume of the fluid contained in V. Define the porosity ϕ by

$$\phi=\frac{V_{\mathrm{f}}}{V}. \tag{12}$$

In general, $\phi=\phi(\vec{x},t)$. Based on eqs. (10)–(12), the relationship between bulk averages and phase averages can be expressed as

$$\left\langle G^{\mathrm{f}}\right\rangle=\phi\overline{G}^{\mathrm{f}}. \tag{13}$$

The definitions of bulk averages and phase averages are similar for functions related to the solid.

Moreover, the law of bulk averages demonstrates the relationship between the averages of the derivatives of variables (time or space domain) and the derivatives of averages (Whitaker, 1999; Fan and Zhu, 2005).

(1) Bulk averages 1: The relation between the time derivative of the average and the average of the time derivative is (Fan and Zhu, 2005; Whitaker, 1999):

$$\partial_t\left\langle G^f\right\rangle=\left\langle\partial_t G^f\right\rangle+\frac{1}{V}\int_{A_{\mathrm{fs}}}G^f\vec{v}^f\cdot\vec{n}\mathrm{d}A, \tag{14}$$

where A_{fs} is the interface between the fluid and solid, $\vec{v}^f$is the fluid velocity at the interface of the fluid and solid, $\vec{n}$ is the unity vector of normal direction at the interface of the fluid and solid, pointing outward from the solid.

(2) Bulk averages 2: The relation between the spatial derivative of the average and the average of the spatial derivative is (Fan and Zhu, 2005):

$$\left\langle \partial_i G^{\mathrm{f}} \right\rangle = \partial_i \left\langle G^{\mathrm{f}} \right\rangle + \frac{1}{V}\int_{A_{\mathrm{fs}}} G^{\mathrm{f}} n_i \mathrm{d}A, \tag{15}$$

where ∂_i represents $\frac{\partial}{\partial x_i}$ and n_i is the ith component of the unit vector of normal direction.

Taking $G^{\mathrm{f}} = 1$ in eq. (15), one obtains (Whitaker, 1999):

$$\partial_i \phi = -\frac{1}{V}\int_{A_{\mathrm{fs}}} n_i \mathrm{d}A. \tag{16}$$

(3) Bulk averages 3: The relation between the divergence of the average and the average of the divergence is (Whitaker, 1999; Fan and Zhu, 2005):

$$\langle \nabla \cdot \bar{\psi} \rangle = \nabla \cdot \langle \bar{\psi} \rangle + \frac{1}{V}\int_{A_{\mathrm{fs}}} \psi_k n_k \mathrm{d}A, \tag{17}$$

where $\bar{\psi}$ is a differentiable vector-valued function, ψ_k is the kth component of the vector $\bar{\psi}$.

2.2 "Complete Biot's theory" in porous medium equation

The following four basic assumptions in porous media are used in derivation of corresponding equations.

Assumption (1): Both the fluid and solid may be viewed as homogeneous on a scale much larger than the characteristic pore size and much smaller than the wavelength of the seismic wave. Thus, for either the fluid phase or the solid phase, over the sub-region volume, medium parameters such as densities of the fluid and solid as well as porosity may be taken approximately as constants.

Assumption (2): Both the fluid and solid are isotropic, and the thermodynamic effect can be ignored.

Assumption (3): Both the fluid and solid are in equilibrium before the seismic wave arrives.

Assumption (4): The porosity gradient in the medium is approximately zero on a scale several times larger than the size of V before the seismic wave arrives.

Assumptions (1) and (2) together imply that the ratio of the fluid area of the cross-section in any volume and the total volume is the porosity (Pride et al., 1992). Under the stated assumptions, the macroscopic motion equations for solid and fluid can be obtained by applying the volume theories (14), (15) and (17) to the microscopic eqs. (4), (5), (8) and (9) (De la Cruz and Spanos, 1985; Spanos, 2001)

$$\frac{\rho_{\mathrm{s}} - \rho_{\mathrm{s}}^{0}}{\rho_{\mathrm{s}}^{0}} - \frac{\phi - \phi_0}{1-\phi_0} + \nabla \cdot \bar{\mathbf{u}}^{\mathrm{s}} = 0, \tag{18}$$

$$\frac{1}{\rho_{\mathrm{f}}^{0}}\frac{\partial \rho_{\mathrm{f}}}{\partial t} + \frac{1}{\phi_0}\frac{\partial \phi}{\partial t} + \nabla \cdot \bar{\mathbf{v}}^{\mathrm{f}} = 0, \tag{19}$$

$$\frac{1}{K_{\mathrm{s}}} p^{\mathrm{s}} = -\nabla \cdot \bar{\mathbf{u}}^{\mathrm{s}} + \frac{\phi - \phi_0}{1-\phi_0}, \tag{20}$$

$$\frac{1}{K_{\mathrm{f}}} p^{\mathrm{f}} = -\nabla \cdot \bar{\mathbf{u}}^{\mathrm{f}} - \frac{1}{\phi_0}\frac{\partial \phi}{\partial t}, \tag{21}$$

$$\begin{aligned}\rho_{\mathrm{s}} \frac{\partial^2}{\partial t^2}\bar{\mathbf{u}}^{\mathrm{s}} &= K_{\mathrm{s}} \nabla (\nabla \cdot \bar{\mathbf{u}}^{\mathrm{s}}) - \frac{K_{\mathrm{s}}}{1-\phi_0}\nabla \phi \\ &+ \frac{\mu_{\mathrm{f}}}{\kappa}\frac{{\phi_0}^2}{1-\phi_0}(\bar{\mathbf{v}}^{\mathrm{f}} - \bar{\mathbf{v}}^{\mathrm{s}}) - \frac{\rho_{12}}{1-\phi_0}\frac{\partial}{\partial t}(\bar{\mathbf{v}}^{\mathrm{f}} - \bar{\mathbf{v}}^{\mathrm{s}}) \\ &+ \frac{\mu_M}{1-\phi_0}\left[\nabla^2 \bar{\mathbf{u}}^{\mathrm{s}} + \frac{1}{3}\nabla (\nabla \cdot \bar{\mathbf{u}}^{\mathrm{s}})\right],\end{aligned} \tag{22}$$

$$\begin{aligned}&\rho_{\mathrm{f}} \frac{\partial^2}{\partial t^2}\bar{\mathbf{u}}^{\mathrm{f}} = -\nabla \bar{p}^{\mathrm{f}} \\ &+ \left[\mu_{\mathrm{f}} \nabla^2 \bar{\mathbf{u}}^{\mathrm{f}} + \left(\xi_{\mathrm{f}} + \frac{1}{3}\mu_{\mathrm{f}}\right)\nabla (\nabla \cdot \bar{\mathbf{u}}^{\mathrm{f}})\right] + \frac{\xi_{\mathrm{f}}}{\phi_0}\nabla \frac{\partial \phi}{\partial t} \\ &+ \frac{1-\phi_0}{\phi_0}\mu_{\mathrm{f}}\left(\frac{\mu_M}{\mu_{\mathrm{s}}(1-\phi_0)} - 1\right)\left[\nabla^2 \frac{\partial \bar{\mathbf{u}}^{\mathrm{s}}}{\partial t} + \frac{1}{3}\nabla\left(\nabla \cdot \frac{\partial \bar{\mathbf{u}}^{\mathrm{s}}}{\partial t}\right)\right] \\ &- \frac{\mu_{\mathrm{f}}\phi_0}{\kappa}(\bar{\mathbf{v}}^{\mathrm{f}} - \bar{\mathbf{v}}^{\mathrm{s}}) + \frac{\rho_{12}}{\phi_0}\frac{\partial}{\partial t}(\bar{\mathbf{v}}^{\mathrm{f}} - \bar{\mathbf{v}}^{\mathrm{s}}).\end{aligned} \tag{23}$$

In addition, Spanos (2001) introduced the porosity equation

$$\frac{\partial \phi}{\partial t} = \delta_{\mathrm{s}} \nabla \cdot \bar{\mathbf{v}}^{\mathrm{s}} - \delta_{\mathrm{f}} \nabla \cdot \bar{\mathbf{v}}^{\mathrm{f}}, \tag{24}$$

where ${\rho_{\mathrm{s}}}^{0}$ and ${\rho_{\mathrm{f}}}^{0}$ represent the densities of the solid and fluid at initial state before the arrival of the wave; ϕ is the porosity and ϕ_0 is the initial porosity before the arrival of the wave; $\bar{\mathbf{u}}^{\mathrm{s}}$ and $\bar{\mathbf{u}}^{\mathrm{f}}$ refer to the average values of the displacements over the volume V of the solid and fluid particles, respectively; $\bar{\mathbf{v}}^{\mathrm{s}}$ and $\bar{\mathbf{v}}^{\mathrm{f}}$ represent the average values of the velocities of the solid and fluid, respectively; p^{s} and p^{f} refer to the pressures in the solid phase and fluid phase, respectively; K_{s} and K_{f} are respectively the bulk modulus of solid and fluid; ξ_{f} refers to the bulk viscosity of the fluid; μ_{s} is the shear modulus of solid; κ is the permeability of the medium; ρ_{12} is the coupling density of solid and fluid; δ_{s} and δ_{f} are flexibility of solid and fluid, respectively (Quiroga-Goode et al., 2005). The subscript and superscript of "s" and "f" in physical variables refer to the solid and fluid, respectively. A bar above a variable means the average value of the variable over the averaging volume V.

3. Time-varying characteristics of porosity and permeability in tight oil and gas media

The tight oil and gas reservoir has special properties in its geological characteristics, the skeleton and saturated fluid, as compared to general two-phase media. Firstly, the porosity of tight reservoirs is small, which is generally less than 0.15 (Wang, 2016). Moreover, tight reservoirs have low permeability, typically on the order of less than milli-darcy (Wang, 2013). The bulk modulus of the skeleton in tight reservoirs is

nearly two orders of magnitude higher than that of the pore fluid (Schon, 2011). Taking these features into consideration, it is possible to simplify the existing porous theory, leading to simpler governing equations in tight oil and gas media. In this section, we will analyze the rate of change of porosity and permeability with respect to time.

The relative motion will occur between the fluid phase and the solid phase due to pressure gradient resulting from the disturbance of passing waves. The motion of the fluid in microscopic pores induced by the pressure difference due to the passing waves in seismic frequency band is assumed to satisfy the Poiseuille flow in circular pipes. Then the relation between the permeability and the porosity is (Carman, 1961; Mavko et al., 1998):

$$\kappa(x,t)=\frac{B\phi^3(x,t)d^2}{(1-\phi(x,t))^2}, \tag{25}$$

where $\kappa(x, t)$ represents the permeability, $\phi(x, t)$ refers to the porosity, both are allowed to depend on the temporal and spatial variables. This relation is known as the Kozeny-Carman equation. The coefficient B is related to tortuosity, and d is the diameter of the solid particles in tight rocks.

The relationship between the change rates of porosity and permeability with time can be obtained by differentiating eq. (25) with respect to time,

$$\frac{1}{\phi(x,t)}\frac{\partial\phi(x,t)}{\partial t}=\frac{1-\phi(x,t)}{3-\phi(x,t)}\frac{1}{\kappa(x,t)}\frac{\partial\kappa(x,t)}{\partial t}. \tag{26}$$

For tight oil and gas media, $\phi(x, t) \in (0, 0.15]$. Thus,

$$\frac{1}{\phi(x,t)}\left|\frac{\partial\phi(x,t)}{\partial \mathrm{t}}\right|<\frac{1}{3}\frac{1}{\kappa(x,t)}\left|\frac{\partial\kappa(x,t)}{\partial \mathrm{t}}\right|. \tag{27}$$

The left-hand side of the inequality (27) represents the relative time rate of change of porosity, while the right-hand side describes the relative time rate of change of permeability. A derivation of eq. (27) is provided in the Appendix online (http://link.springer.com). A physical interpretation of eq. (27) is that the relative time change rate of porosity and the relative time change rate of permeability are on the same order of magnitude.

The study of change rate of permeability has important theoretical significance and practical values in applications. In particular, the permeability change of a fractured rock under external forces has attracted extensive attention. It has been a long time to study the static change of permeability in porous media and many kinds of rock samples have been measured. In recent years, the dynamic change of permeability under excitation has attracted wide attention (Yang et al., 2008; Zheng et al., 2019; Zheng and Liu, 2019). Yang et al. (2008) studied the time-varying characteristics of permeability of core measurements in tight reservoirs and their experimental results indicate that

$$\left|\frac{1}{\kappa(x,t)}\frac{\partial\kappa(x,t)}{\partial t}\right|<10^{-12}. \tag{28}$$

In the inequality (28), the rate of relative change of permeability with respect to time is expressed in Hz. Combining eq. (28) with eq. (27), we see that the absolute rate of porosity with time satisfies

$$\left|\frac{\partial\phi(x,t)}{\partial t}\right|<10^{-13}. \tag{29}$$

In this section, we studied the rate of porosity with time in tight reservoirs based on the measurement of relative time-varying characteristic of the permeability, where the pore fluid motion is assumed a Poiseuille flow. The results show that the rate of time change of porosity is less than 10^{-13} in size for tight oil and gas reservoirs. The amplitude of oscillation of the particle due to the passing waves is of the order of 10^{-6} (Chen et al., 2009), and the induced pressure is much less than MPa. Thus, we speculate that the rate of change in the permeability and the porosity with respect to time due to this pressure is much less than the measured values given by Yang et al. (2008). We assume that the change of the porosity induced by the seismic wave is a continuous function of time. When seismic wave propagates in the tight oil or gas media, the induced time-varying rate of the porosity is negligible. This finding directly leads us to an assumption for the tight media. Assumption (5): the porosity is independent of time.

It is therefore deduced that the corresponding second-order time derivative of porosity equals zero.

4. Seismic wave equations for tight oil/gas sandstone media

We apply the divergence operation to eqs. (22) and (23), and make use of eqs. (18)–(21) and (24), as a result, an equation coupling the porosity and the pressure is obtained

$$\frac{\rho_{\phi\mathrm{f}}}{\phi_0}\left(\frac{\partial^2\phi}{\partial t^2}+2a_{\phi\mathrm{f}}\frac{\partial\phi}{\partial t}-2b_{\phi\mathrm{f}}\nabla^2\frac{\partial\phi}{\partial t}\right)$$
$$=-\frac{\rho_{p\mathrm{f}}}{K_{\mathrm{f}}}\left(\frac{\partial^2 p^{\mathrm{f}}}{\partial t^2}+2a_{p\mathrm{f}}\frac{\partial p^{\mathrm{f}}}{\partial t}-2b_{p\mathrm{f}}\nabla^2\frac{\partial p^{\mathrm{f}}}{\partial t}-v_{p\mathrm{f}}^2\nabla^2 p^{\mathrm{f}}\right), \tag{30}$$

where

$$a_{\phi\mathrm{f}}=\frac{1}{2}\frac{\mu_{\mathrm{f}}\phi_0(\alpha_1+1)}{\kappa\rho_{\phi\mathrm{f}}}, \tag{31}$$

$$b_{\phi\mathrm{f}}=\frac{2}{3}\frac{\mu_{\mathrm{f}}-\alpha_1\sigma_M/\phi_0}{\rho_{\phi\mathrm{f}}}, \tag{32}$$

$$\rho_{\phi\mathrm{f}}=\rho_{\mathrm{f}}-\rho_{12}(\alpha_1+1), \tag{33}$$

$$a_{p\mathrm{f}}=\frac{1}{2}\frac{\mu_{\mathrm{f}}\phi_0(\alpha_2-1)}{\kappa\rho_{p\mathrm{f}}}, \tag{34}$$

$$b_{pf}=\frac{1}{2\rho_{pf}}\left[\xi_f+\frac{4}{3}\left(\mu_f-\frac{\sigma_M}{\phi_0}\alpha_2\right)\right], \tag{35}$$

$$v_{pf}^2=\frac{K_f}{\rho_{pf}}. \tag{36}$$

In eq. (30), $\rho_{pf}=\rho_f-\frac{\rho_{12}}{\phi_0}(\alpha_2-1)$, $\alpha_1=\frac{\phi_0-\delta_f}{\delta_s}$, $\alpha_2=\frac{\delta_f}{\delta_s}$, $\sigma_M=(1-\phi_0)\mu_f\left[\frac{\mu_M}{(1-\phi_0)\mu_s}-1\right]$, $\mu_M=(1-\phi_0)\mu_s(1+c)$, c is a constant.

For tight oil and gas media, $\frac{\rho_{\phi f}}{\phi_0}$ and $2a_{\phi f}\frac{\rho_{\phi f}}{\phi_0}$ are much larger than 10^{-13}. Assumptions 2 and 4 in section 2.2 imply $\nabla^2\frac{\partial\phi}{\partial t}\approx 0$. Assumption 5 in section 3 manifests $\frac{\partial^2\phi}{\partial t^2}\approx 0$. Use these relations in eq. (30) to obtain approximately that

$$\frac{\partial^2 p^f}{\partial t^2}+2a_{pf}\frac{\partial p^f}{\partial t}-2b_{pf}\nabla^2\frac{\partial p^f}{\partial t}-v_{pf}^2\nabla^2 p^f=0. \tag{37}$$

Recall the diffusive-viscous wave equation (Korneev et al., 2004; Zhao et al., 2014a, 2014b)

$$\frac{\partial^2 p^f}{\partial t^2}+\gamma\frac{\partial p^f}{\partial t}-\eta\nabla^2\frac{\partial p^f}{\partial t}-v^2\nabla^2 p^f=0, \tag{38}$$

where γ and η are diffusive and viscous attenuation coefficients, respectively; v is the wave propagation velocity in a nondispersive media. We note that eqs. (37) and (38) are completely consistent in form. For a tight oil and gas medium, the governing equation of the wave has the same form as that of the diffusive-viscous wave equation, but the coefficient of the equation can be determined by the physical parameters of the medium. The diffusive-viscous wave equation can be applied to explain the seismic low frequency shadow phenomena (Goloshubin and Korneev, 2000; He et al., 2008). One of the contributions of this paper is to relate the parameters γ, η in eq. (38) to observable physical quantities in the diffusive-viscous wave equation in tight oil and gas media, i.e. $\gamma=2a_{pf}$, $\eta=2b_{pf}$ and $v^2=v_{pf}^2$. In this section, we have demonstrated that eq. (30) can be simplified to eq. (37) for a tight oil and gas media based on the physical principal and the range of the physical parameters in tight rocks. In the next section, we will compare the difference between the results of eqs. (30) and (37) through numerical simulation to verify the simplification. The well-posedness of initial-boundary value problems for eq. (37) or eq. (38) has been addressed in Han et al. (2020).

5. Numerical examples

In this section, we report numerical simulation results on wave propagation in tight reservoirs, using the finite-element software COMSOL Multiphysics. We will first study the seismic wave response characteristics of tight reservoirs through numerical simulations using eqs. (30) and (37). Then, we will study the reflection and transmission characteristics of seismic waves induced by a highly attenuating tight layer sandwiched in a low attenuating background using eq. (37). In all numerical simulations, the source is a Ricker wavelet with a central frequency of 20 Hz and a time delay of 0.05 s. The amplitude of the force source is 10^5 N. Since the spatial domain is unbounded, we use a perfectly matched layer (PML) to truncate the physical region and to prevent artificial reflections (He et al, 2019, 2020). The PML contains 10 layers of grids. For spatial discretization, meshes with square elements are adopted for the whole model including the PML domain. We employ second-order polynomials to interpolate the functions on each node. For time integration, we use the generalized α method, which is similar to the second-order backward finite difference scheme. It is the default solver for wave problems in the software and it can effectively avoid the stability issue during numerical simulation. To ensure solution accuracy, the time step is selected according to the criterion of CFL<0.4.

5.1 Validation model

We consider the seismic wave propagation in a gas saturated tight reservoir to illustrate the usefulness of the proposed theory. The physical domain has a dimension of 1000 m × 1000 m and is surrounded by PML. The material parameters are chosen to be a_{pf} =5 Hz, b_{pf}=0.028 m^2 s^{-1}, v_{pf}=2000 m s^{-1}, μ_f =2.2×10^{-4} Poise, κ=0.001D. During the simulation, the source is placed at the center of the model, and the source-receiver distance is 550 m. Eqs. (30) and (37) are solved separately and we show the results of the two cases in Figure 1. The difference between the two results is insignificant. Therefore, for this example, the contribution of the first-order time derivative of the porosity in eq. (30) has little influence on the results, illustrating the usefulness of our simplification for the model.

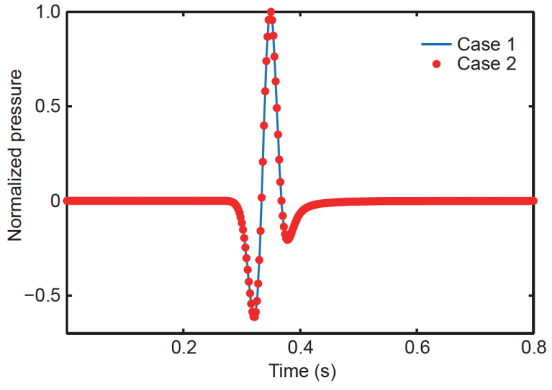

Figure 1 Seismic response in tight gas medium. Case 1 corresponds to the result using eq. (30) and Case 2 corresponds to the result using eq. (37).

5.2 Single inter-layer model

In this section, we consider the interaction between seismic waves and a horizontally isotropic thin layer embedded in a background medium. The model configuration is shown in Figure 2. The background medium has the same material parameters as those in Section 5.1. The attenuation property of the interlayer is adjusted by varying the value of a_{pf}. The vertical distance between the source and the upper surface of the tight reservoir is l_1 = 300 m. The source parameters are kept unchanged. Two arrays of receivers were placed in the model to record seismic signals. The vertical distances from the receivers at the top and bottom to the center of the model are 1200 and 800 m, respectively.

We consider two cases to analyze the seismic response induced by the tight layer. In the first case, we analyze the influence of the reservoir attenuation characteristics on seismic wave propagation by varying the value of viscous coefficients while keeping the layer thickness h unchanged. In the second case, we investigate the influence of the layer thickness where the attenuation property in the tight reservoir remains unchanged. For simulations, we place two receivers at (300 m, 200 m) and (300 m, −200 m) to record seismic signals. The results are shown in Figure 3. In Figure 3a, we can observe the direct wave, which is not affected by the sandwiched layer. We observe reflected seismic waves at approximately 0.36 s. The amplitude of the reflected wave is significantly influenced by the attenuating properties of the sandwiched layer. The amplitude of the reflected signal becomes larger for a smaller value of the viscous coefficient a_{pf} inside the layer. It should be noted that the viscous property of the background media is kept unchanged during simulations. When a_{pf} inside the sandwiched layer increases, the attenuation of the layer becomes stronger, resulting in a more intensive reflected signal. Another important observation is on the influence of the layer attenuation on the transmitted wave. An increase in the attenuation of the layer reduces the amplitude of the transmitted waves. Note that all signals in Figure 3 are normalized for the convenience of analysis and comparison.

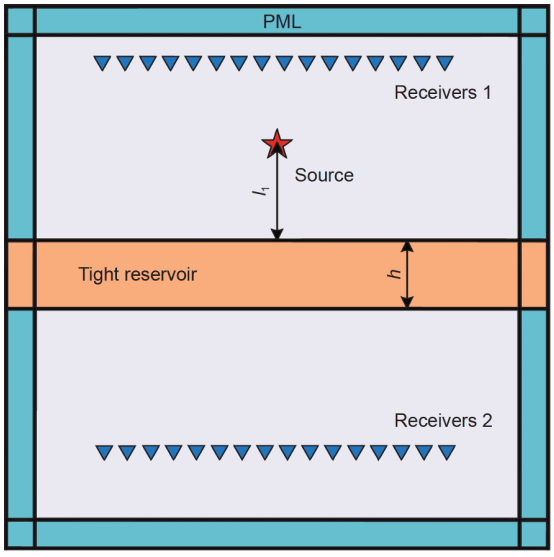

Figure 2 Configurations of numerical simulation for the single inter-layer model.

We perform similar simulations to investigate the influence of the layer thickness on seismic reflection and transmission. The material properties of the background and the layer are the same as previously. We study the seismic response by varying the layer thickness h from 10 to 40 m. The simulated results are shown in Figure 4. One can see that the layer thickness has a similar influence to that of the viscous coefficient on seismic reflection. An increase in the layer thickness results in a stronger reflected wave. In addition, the layer thickness has a significant effect on the phase of the reflected wave, for the combined effect of the layer attenuation and thin-layer tuning. The layer thickness also influences the amplitude of the transmitted waves, but it has no significant influence on the phase. The transmitted wave has a smaller amplitude for a thinner layer.

It is important to study the characteristic of seismic signals changing with the offset distance, which is a key content in seismic exploration. During the simulation, properties of the background medium are kept unchanged; the thickness of the embedding layer is 60 m; and the viscous coefficient of the

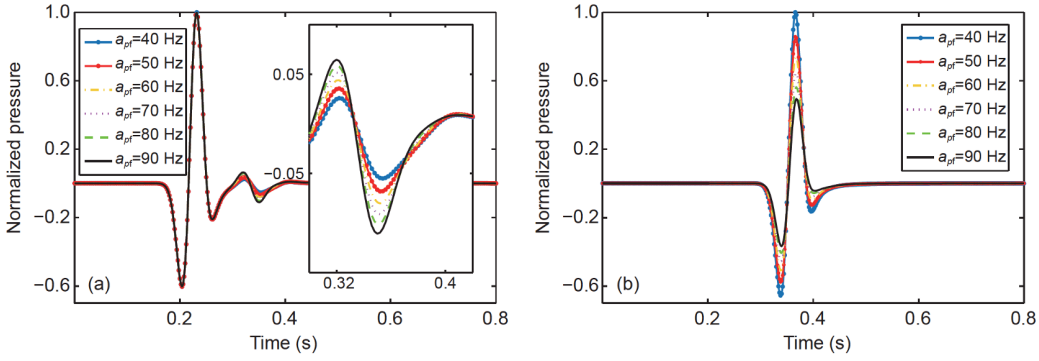

Figure 3 Influence of a_{pf} on seismic signals for the single inter-layer model. (a) Direct and reflected seismic signals and (b) transmitted seismic signals.

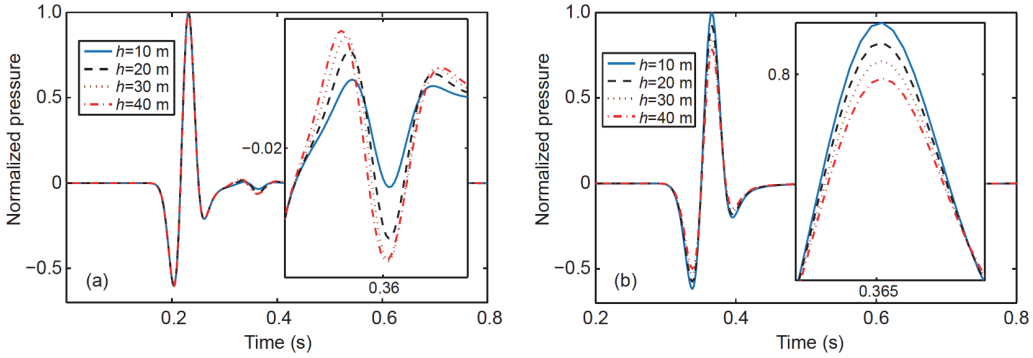

Figure 4 Influence of h on seismic signals for the single inter-layer model. (a) Direct and reflected seismic signals and (b) transmitted seismic signals.

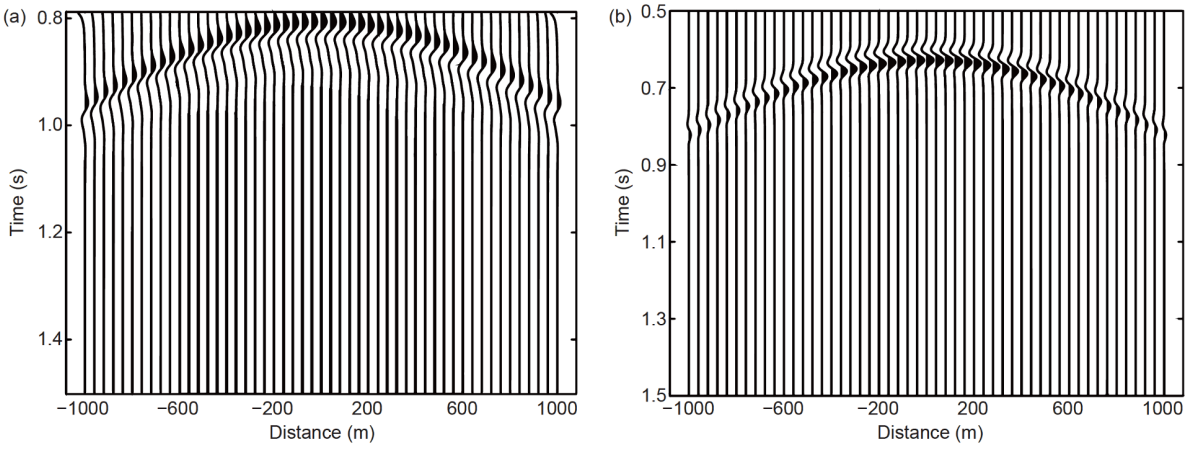

Figure 5 Synthetic seismograms for the single inter-layer model. (a) Reflected seismic signals and (b) transmitted seismic signals.

reservoir is a_{pf} = 60 Hz. We depict the synthetic seismogram of the signals recorded by the receivers in Figure 5. The direct wave signals are not presented in the synthetic seismogram due to their much larger amplitudes. Since only a single thin layer exists in the model, one can spot only one reflected wave (see Figure 5a) and one transmitted wave (see Figure 5b). The amplitude of the seismic reflected wave and the transmitted wave decreases with the increase of offset. It should be noted that the reflected signals are mainly caused by the attenuation characteristic of the embedding layer in this model. We observe that the amplitude of reflected signals varies slowly with offset when the offset is small. For large offset, the transmitted signal varies significantly.

5.3 Heterogeneous inter-layer model

In Section 5.2, based on a single inter-layer model, we analyze properties of seismic reflection and transmission for different viscous coefficients, layer thickness and offset. In this section, we consider the heterogeneity of the sandwich layer to investigate whether seismic wave can reflect the lateral heterogeneity of the reservoir. The model configurations are shown in Figure 6. Three tight layers denoted by A, B and C are sandwiched in a background medium. All layers have the same thickness h = 60 m. The horizontal length of the layer B is l_2 = 1300 m. The material parameters of the

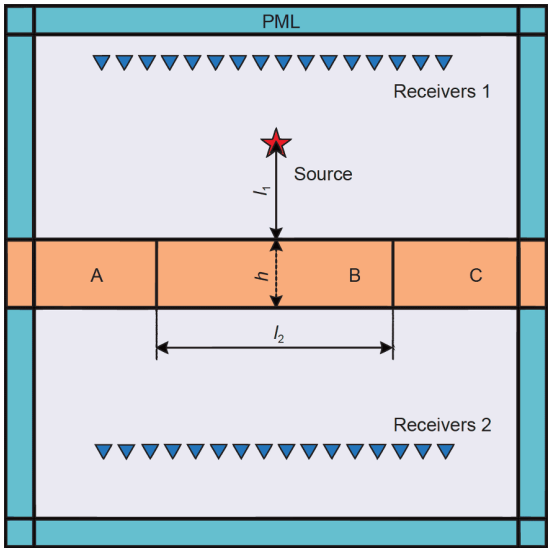

Figure 6 Configurations of numerical simulation for the heterogeneous inter-layer model.

background and the embedding layer are shown in Table 1 (Zhao et al., 2014a). The vertical distance between the source and the center of the model is 600 m, and they are 1200 and 600 m for receivers 1 and 2, respectively. Other data for the simulation setting are the same as those in Section 5.2.

Figure 7 shows snapshots of the simulated wave field. Figure 7a corresponds to the reflected and transmitted waves generated after the pressure wave impinging layer B at the time 0.7 s, and the situation is similar to that in Section 5.2. As the time increases to 1 s, the reflected, transmitted as well as scattered waves are shown in Figure 7b. Figure 7c shows the situation at the time 1.21 s. Since the thickness of the sandwiched layer A is larger than the wavelength, multiple scattering waves can be observed and they propagate gradually to the far field over the time, as shown in Figure 7d. These scattering waves provide the possibility for the lateral heterogeneity detection of tight reservoirs.

In Figure 8, we present the synthetic seismograms recorded by the two arrays of receivers. In Figure 8a, the amplitude of the reflected seismic signal has a maximum value when the offset is 0 m and it decreases gradually with the increase of the offset distance. In addition, the wavelength of seismic signals changes with the offset increasing from −1400 to 1400 m. Another important observation is the scattered waves occurring at the position of sandwiched layer A. The scattering waves corresponding to the position of layer C were not observed due to their rather small amplitudes. For the result in Figure 8b, one can observe the scattered waves in addition to the transmitted wave. We can locate the interface between A and B as well as that between B and C by carefully processing the scattering waves. The scattered waves are not observable in the synthetic seismogram due to their small amplitudes. This model clearly shows that the seismic signal contains information of lateral heterogeneity of the reservoir, which provides a theoretical basis for well positioning.

6. Conclusion and discussion

Based on the complete Biot's theory and experimental results, we derived the wave equations for tight oil/gas media

Table 1 Material parameters for the heterogeneous inter-layer model (Zhao et al., 2014a)

Medium	Velocity ($m\ s^{-1}$)	Density ($kg\ m^{-3}$)	Viscous coefficient (Hz)	Diffusive coefficient ($m^2\ s^{-1}$)
Background	1190	1800	10	0.056
Layer A	630	140	15	0.008
Layer B	1015	800	90	0.2
Layer C	1470	2100	56	0.056

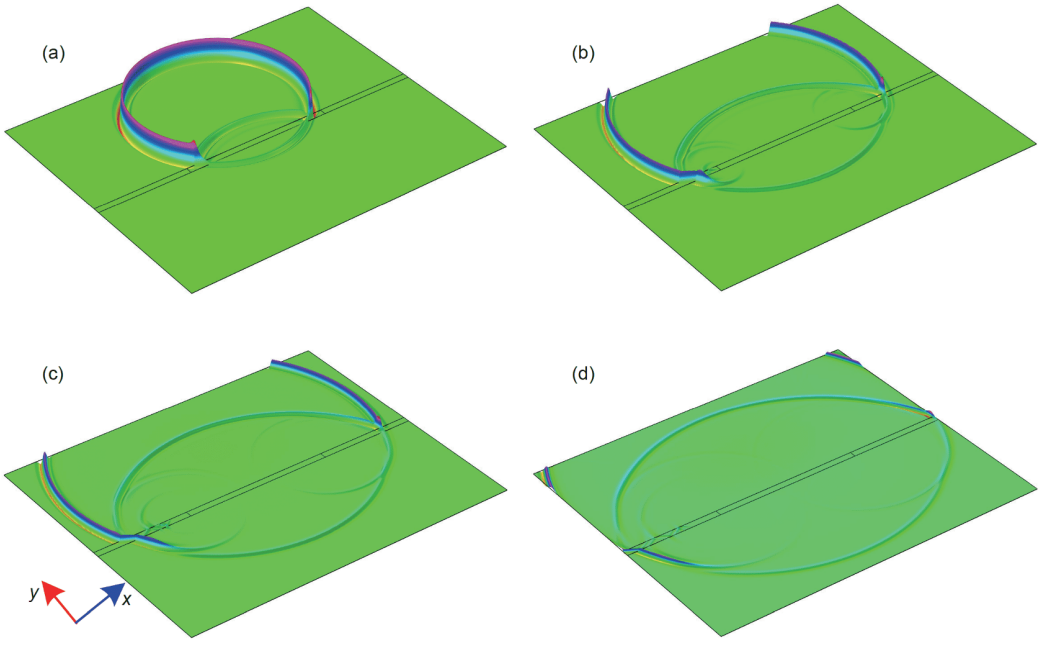

Figure 7 Snapshots of pressure distribution for the heterogeneous inter-layer model. (a) 0.7 s, (b) 1.0 s, (c) 1.21 s, (d) 1.4 s.

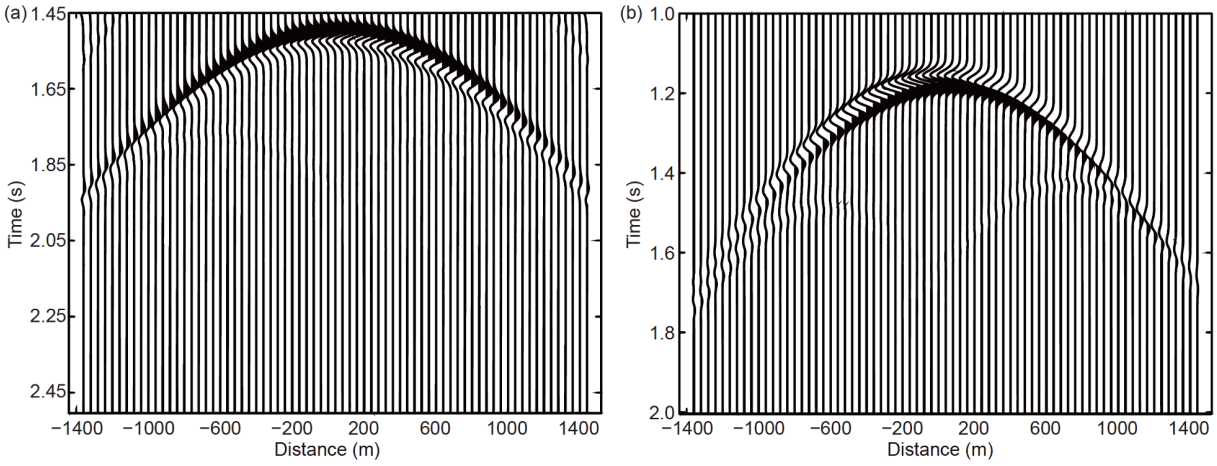

Figure 8 Synthetic seismograms for the heterogeneous inter-layer model. (a) Reflected seismic signals and (b) transmitted seismic signals.

under reasonable assumptions (Assumption 5 in the paper) which have the same forms as the diffusive-viscous wave equations. In addition, relations between the coefficients in diffusive-viscous wave equations and the physical parameters are provided as well. It potentially enables us to directly estimate porosity, permeability from seismic data because fewer coefficients are present in the equations. The numerical results demonstrate the usefulness of the proposed equations. Moreover, reflection and transmission properties of the seismic wave passing through tight reservoir model are investigated, which shows that attenuation of the interlayer significantly affects the reflection and transmission. In addition, the seismic wave contains transversal heterogeneity information.

Future work includes testing the derived equations through practical applications, and evaluating the accuracy of the solutions for both forward and inverse problems. Moreover, we need rock physical experiments to verify the applicability of the equations for different tight oil/gas media. If the time-dependent porosity could not be ignored, the machine learning approach would be used to acquire the relationship between fluid pressure and porosity variation, which is important for refining the theory in porous media. In this paper, the media are assumed to be isotropic, which is not satisfactory if the goal is to completely characterize the actual cases. Therefore, we will extend our work for the anisotropic case. In addition, we do not consider the temperature effect in this paper. Since the fluid bulk modulus and viscosity are sensitive to the temperature, we will consider the tight oil/gas wave equations for the coupled thermo-elastic case, which is significant for the deep hydrocarbon exploration.

Acknowledgements *The work was supported by the National Natural Science Foundation of China (Grant Nos. 41390450, 41390454, 91730306), the National Science and Technology Major Projects (Grant Nos. 2016ZX05024-001-007, 2017ZX05069), and the National Key R & D Program of the Ministry of Science and Technology of China (Grant No. 2018YFC0603501).*

References

Biot M A. 1956a. Theory of propagation of elastic waves in a fluid-saturated porous solid. I. Low-frequency range. J Acoust Soc Am, 28: 168–178

Biot M A. 1956b. Theory of propagation of elastic waves in a fluid-saturated porous solid. II. Higher frequency range. J Acoust Soc Am, 28: 179–191

Biot M A. 1962. Generalized theory of acoustic propagation in porous dissipative media. J Acoust Soc Am, 34: 1254–1264

Biot M A. 1973. Nonlinear and semilinear rheology of porous solids. J Geophys Res, 78: 4924–4937

Bourbié T, Coussy O, Zinszner B. 1987. Acoustics of Porous Media. Houston: Gulf Publishing Co.

Carman P C. 1961. Lecoulement des GazaTravers les Milieux Poreux, Bibliothéque des Sciences et Techniques Nucleaires. Paris: Presses Universitaires de France

Chen Y, Huang T F, Liu E R. 2009. Rock Physics Handbook (in Chinese). Hefei: University of Science and Technology of China Press

Cheng Y F, Yang D H, Yang H Z. 2002. Biot/squirt model in viscoelastic porous media. Chin Phys Lett, 19: 445–448

Cruz V D L, Sahay P N, Spanos T J T. 1993. Thermodynamics of porous media. Proc R Soc Lond A, 443: 247–255

de la Cruz V, Spanos T J T. 1985. Seismic wave propagation in a porous medium. Geophysics, 50: 1556–1565

de la Cruz V, Spanos T J T. 1989. Seismic boundary conditions for porous media. J Geophys Res, 94: 3025–3029

Diallo M S, Appel E. 2000. Acoustic wave propagation in saturated porous media: Reformulation of the Biot/Squirt flow theory. J Appl Geophys, 44: 313–325

Diallo M S, Prasad M, Appel E. 2003. Comparison between experimental results and theoretical predictions for P-wave velocity and attenuation at ultrasonic frequency. Wave Motion, 37: 1–16

Fan L S, Zhu C. 2005. Principles of Gas-Solid Flows. Cambridge: Cambridge University Press

Fung Y. 1994. A first Course in Continuum Mechanics. 3rd ed. New Jersey: Prentice-Hall, Inc.

Goloshubin G M, Korneev V A. 2000. Seismic low-frequency effects from fluid-saturated reservoir. In: Proceedings SEG Meeting (Calgary), 70th Annual International Meeting, SEG. Expanded Abstracts. 1671−1674

Han W, Gao J, Zhang Y, Xu W. 2020. Well-posedness of the diffusive-viscous wave equation arising in geophysics. J Math Anal Appl, 486: 123914

He Y, Chen T, Gao J. 2019. Unsplit perfectly matched layer absorbing boundary conditions for second-order poroelastic wave equations. Wave Motion, 89: 116–130
He Y, Chen T, Gao J. 2020. Perfectly matched absorbing layer for modelling transient wave propagation in heterogeneous poroelastic media. J Geophys Eng, 17: 18–34
He Z, Xiong X, Bian L. 2008. Numerical simulation of seismic low-frequency shadows and its application. Appl Geophys, 5: 301–306
Hickey C J, Spanos T J T, Cruz V. 1995. Deformation parameters of permeable media. Geophys J Int, 121: 359–370
Johnston D H, Toksöz M N, Timur A. 1979. Attenuation of seismic waves in dry and saturated rocks: II. Mechanisms. Geophysics, 44: 691–711
Kang Y. 2016. Resource potential of tight sand oil & gas and exploration orientation in China (in Chinese). Nat Gas Industry, 36: 10−18
Korneev V A, Goloshubin G M, Daley T M, Silin D B. 2004. Seismic low-frequency effects in monitoring fluid-saturated reservoirs. Geophysics, 69: 522–532
Landau L D, Lifshitz E M. 1959. Elasticity Theory. Oxford: Pergamon Press
Landau L D, Lifshitz E M. 1987. Fluid Mechanics. 2nd ed. Oxford: Pergamon Press
Mase G T, Mase G E. 2001. Continuum Mechanics for Engineers. 2nd ed. Boca Raton: CRC Press
Mavko G, Mukerji T, Dvorkin J. 1998. Rock Physics Handbook: Tools for Seismic Interpretation in Porous Media. Cambridge: Cambridge University Press
Parra J O. 1997. The transversely isotropic poroelastic wave equation including the Biot and the squirt mechanisms: Theory and application. Geophysics, 62: 309–318
Pride S R, Gangi A F, Morgan F D. 1992. Deriving the equations of motion for porous isotropic media. J Acoust Soc Am, 92: 3278–3290
Quiroga-Goode G, Jiménez-Hernández S, Pérez-Flores M A, Padilla-Hernández R. 2005. Computational study of seismic waves in homogeneous dynamic-porosity media with thermal and fluid relaxation: Gauging Biot theory. J Geophys Res, 110: B07303
Sahay P N. 2001. Dynamic Green's function for homogeneous and isotropic porous media. Geophys J Int, 147: 622–629
Sahay P N, Spanos T J, De la Cruz V. 2000. Macroscopic constitutive equations of an inhomogeneous and anistropic porous medium by volume averaging approach. SEG Technical Program Expanded Abstracts. 1834–1837
Sams M S, Neep J P, Worthington M H, King M S. 1997. The measurement of velocity dispersion and frequency-dependent intrinsic attenuation in sedimentary rocks. Geophysics, 62: 1456–1464
Schon J H. 2011. Physical Properties of Rocks. A workbook. Elsevier. 158
Spanos T J. 2001. The Thermophysics of Porous Media. Boca Raton: CRC Press
Spanos T J T. 2009. Seismic wave propagation in composite elastic media. Transp Porous Media, 79: 135–148
Spanos T J, Udey N, Dusseault M. 2002. Completing Biot Theory. In: Proceedings 2nd Biot Conf. on Poromechanics. 819−826
Wang D. 2016. Study on the rock physics model of gas reservoirs in tight sandstone (in Chinese). Chin J Geophys, 59: 4603−4622
Wang Z. 2013. Research progress, existing problem and development trend of tight rock oil (in Chinese). Petrol Geol Exper, 35: 7−15
Whitaker S. 1999. The Method of Volume Averaging: Theory and Applications of Transport in Porous Media. Dorderecht: Kluwer Academic
Winkler K W. 1985. Dispersion analysis of velocity and attenuation in Berea sandstone. J Geophys Res, 90: 6793–6800
Yang S, Liu W, Feng J, Wang R, Tu Z, Zhang Y, Tang Z, Hang D. 2008. Effect of pressure time on reservoir core permeability (in Chinese). J China Univ Petrol, 32: 0064−0068
Zhao H, Gao J, Liu F. 2014a. Frequency-dependent reflection coefficients in diffusive-viscous media. Geophysics, 79: T143–T155
Zhao H, Gao J, Zhao J. 2014b. Modeling the propagation of diffusive-viscous waves using flux-corrected transport–finite-difference method. IEEE J Sel Top Appl Earth Observ Remote Sens, 7: 838–844
Zhao X, Liao Q. 1983. Mechanics of Viscous Fluids (in Chinese). Beijing: China Machine Press
Zheng L, Liu J. 2019. Variation of seepage in one-dimensional low-permeable layer under low-frequency vibration. J Por Media, 22: 1519–1538
Zheng L, Zhang Y, Li Z, Ma P, Yang X. 2019. Rock consolidation seepage analysis under low frequency fluctuation considering different degree of porosity and pressure (in Chinese). Rock Soil Mech, 40: 1158−1196

(Responsible editor: Xingyao YIN)